*J. Fluid Mech.* (1969), *vol.* 39, *part* 3, *pp.* 611–627
*Printed in Great Britain*



# Stability of plane Poiseuille flow to periodic disturbances of finite amplitude

By C. L. PEKERIS AND B. SHKOLLER†
Department of Applied Mathematics, The Weizmann Institute of Science, Rehovot, Israel

(Received 5 May 1969)

A disturbance of finite amplitude $\lambda$, which is periodic in the direction of the axis of the channel, is superimposed on plane Poiseuille flow, and the subsequent development of the disturbance is studied. The disturbance is represented by an expansion in the eigenfunctions of the Orr–Sommerfeld equation with coefficients which are functions of the time, and an accurate numerical solution of the truncated system of non-linear ordinary differential equations for the coefficients is obtained.

It is found that even for Reynolds numbers $R$ less than the critical value $R_c$, the flow breaks down when $\lambda$ exceeds a critical value $\lambda_c(R)$. This is shown in figure 11 for the case when the initial disturbance is represented by the first mode of the Orr–Sommerfeld equation. The development of this type of disturbance is illustrated in figures 1, 3 and 13 and, for the case of a higher-order mode initial disturbance, in figure 14. Near the time of breakdown, the curvature of the modified mean flow changes sign (figure 15), but a disturbance may die down even after a reversal in the sign of the curvature has taken place (see figure 2).

The stability of plane Poiseuille flow to disturbances of finite amplitude is affected by the characteristics of the higher-order modes of the Orr–Sommerfeld equation. As shown in figures 4, 10, and 12, and in figures 5, 6, and 7, these modes are either of a 'boundary type', characteristic of the region near the wall, or of an 'interior type', characteristic of the centre of the channel. The modes in the transition zone, where the two types merge, are easily amplified through mutual constructive interference, even though individually they have high damping coefficients. It is these transition modes which are mainly responsible for the breakdown through finite amplitude effects.

## 1. Introduction

In the literature on hydrodynamic stability, Landau's (1944) paper stands out. It purports to reveal the essential physical factors controlling the initiation of turbulence. In Landau's picture, the transition into turbulent motion occurs by a succession of perturbations each starting with an initial dynamic instability which, however, does not grow exponentially large, but is braked at a high terminal level by finite amplitude effects. The phases of the perturbation at the

† Present address: Institute for Space Studies, New York City.

termination of each spasm are largely arbitrary, and this phase-indeterminacy he considers to be basic to the statistical nature of turbulent motion. Landau's model naturally has appeal to experts in statistical mechanics. It must be pointed out, however, that in his discussion, which is of a qualitative nature only, Landau does not offer proofs for his assertions. Yet these assertions on turbulence are intriguing, in view of the success with which similar predictions of his have met in many branches of physics.

One approach in gaining insight into the mechanism of the initiation of turbulence is to study numerically disturbances in idealized basic flows, where, however, we can attempt to take full account of the finite-amplitude aspect of the disturbance. In this investigation we start initially with plane Poiseuille flow in the $x$ direction:

$$\left.\begin{aligned} &\bar{u}_0 = \frac{\partial \psi_0}{\partial y} = 1 - y^2, \quad \bar{v}_0 = \frac{\partial \psi_0}{\partial x} = 0 \\ &\psi_0 = y - \tfrac{1}{3}y^3, \quad (-1 \leqslant y \leqslant 1). \end{aligned}\right\} \tag{1}$$

At time $t = 0$ there is superimposed on the plane Poiseuille flow a disturbance of finite amplitude which is periodic in $x$ and of wavelength $(2\pi/\alpha)$. The resulting stream function $\psi$ is given by

$$\psi = \psi_0 + \sum_{n=-\infty}^{\infty} f_n(y,t)\, e^{-in\alpha x}, \tag{2}$$

where, because of the reality conditions, we must have

$$f_{-n}(y,t) = \bar{f}_n(y,t), \tag{3}$$

the bar denoting complex conjugate. The restriction to periodicity of the disturbance in the $x$ direction is of course an artificial one, and practically precludes the possibility of checking the results experimentally. However, under this simplifying assumption, the mathematical problem can be reduced to a system of *ordinary* differential equations whose solution can be achieved without ambiguity as to the accuracy of the results. Certain qualitative features, which these results exhibit, would be expected to apply also to more general types of disturbance. Granted the simplifying assumption of periodicity in the direction of main flow, our aim has been to retain enough of the non-linear terms so as to be able to study the stability in the whole $\alpha$–$R$ plane, rather than only in the vicinity of the apex† of the 'neutral curve', as was done by Stuart (1960), Watson (1960) and Eckhaus (1965).

## 2. Method of solution

When substituted into the Navier–Stokes equation,

$$\frac{\partial \nabla^2 \psi}{\partial t} + \frac{\partial \psi}{\partial y}\frac{\partial \nabla^2 \psi}{\partial x} - \frac{\partial \psi}{\partial x}\frac{\partial \nabla^2 \psi}{\partial y} = \frac{1}{R}\nabla^4 \psi, \tag{4}$$

† The apex of the neutral curve in the $\alpha$–$R$ plane occurs at the point $\alpha_c = 1{\cdot}020548$, $R_c = 5772{\cdot}22$. Near the apex, the neutral curve is given by $R = R_c + 1{\cdot}1 \times 10^5\,(\alpha - \alpha_c)^2 + \ldots$.

(2) leads to (see Eckhaus 1965, p. 98; Watson 1960)

$$f_n^{\mathrm{IV}} - 2\alpha^2 n^2 \ddot{f}_n + \alpha^4 n^4 f_n - R\partial/\partial t(\ddot{f}_n - \alpha^2 f_n) + i\alpha R[(1-y^2+\dot{f}_0)(\ddot{f}_n - \alpha^2 n^2 f_n) + (2-\ddot{f}_0) f_n] = i\alpha R K_n, \quad (5)$$

$$K_n = \sum_{k=1}^{n-1} [k f_k \dot{g}_{n-k} - (n-k)\dot{f}_k g_{n-k}] + \sum_{k=1}^{\infty} [-k\bar{f}_k \dot{g}_{n+k} - (n+k)\dot{\bar{f}}_k g_{n+k} + k\dot{f}_{n+k}\bar{g}_k + (n+k) f_{n+k}\dot{\bar{g}}_k] \quad (n \geqslant 1), \quad (6)$$

where

$$g_n = \ddot{f}_n - \alpha^2 n^2 f_n, \quad (7)$$

and dots signify differentiation with respect to $y$.

The mean flow $\bar{u}(y,t)$ is, from (2), given by

$$\bar{u}(y,t) = (\partial\bar{\psi}/\partial y) = 1 - y^2 + \dot{f}_0(y,t). \quad (8)$$

For $n = 0$, (5) yields

$$f_0^{\mathrm{IV}} - R\frac{\partial}{\partial t}\ddot{f}_0 = 2\alpha R \mathscr{I} \frac{\partial}{\partial y} \sum_{k=1}^{\infty} k\bar{f}_k \ddot{f}_k, \quad (9)$$

where $\mathscr{I}$ denotes the imaginary part. We integrate (9) into

$$\ddot{f}_0 - R\frac{\partial}{\partial t}\dot{f}_0 = 2\alpha R \mathscr{I} \sum_{k=1}^{\infty} k\bar{f}_k \ddot{f}_k. \quad (10)$$

It can be shown (Stuart 1960, Watson 1960) that putting the constant of integration in (10) equal to zero is equivalent to making the assumption that the mean pressure-gradient remains unchanged by the perturbation. This would be realized in practice if the mean pressure is maintained constant both at the intake of the channel and at the outflow.

We shall truncate the expansion (2) at $n = 3$, and will investigate the domain of the variables where the neglect of the truncated terms can be justified. A suitable representation for $\dot{f}_0$, which satisfies the boundary condition of the vanishing of $\dot{f}_0$ at $y = 1$, is:

$$\dot{f}_0(y,t) = \sum_{\sigma=1}^{s} A_\sigma(t) \cos[(\sigma - \tfrac{1}{2})\pi y]. \quad (11)$$

The other functions we expand in terms of the even eigenfunctions $\phi_n^\nu(y)$ of the Orr–Sommerfeld equation,

$$\phi_n^{\nu\mathrm{IV}} - 2\alpha^2 n^2 \ddot{\phi}_n^\nu + \alpha^4 n^4 \phi_n^\nu + i\alpha n R[(1-y^2-c_n^\nu)(\ddot{\phi}_n^\nu - \alpha^2 n^2 \phi_n^\nu) + 2\phi_n^\nu] = 0, \quad (12)$$

$$\nu = 1, 2, \ldots, \quad (13)$$

which satisfy the boundary conditions

$$\phi_n^\nu(1) = \dot{\phi}_n^\nu(1) = \phi_n^\nu(-1) = \dot{\phi}_n^\nu(-1) = 0. \quad (14)$$

The eigenfunctions $\tilde{\phi}_n^\nu(y)$ of the system *adjoint* to (12)

$$\tilde{\phi}_n^{\nu\mathrm{IV}} - 2\alpha^2 n^2 \ddot{\tilde{\phi}}_n^\nu + \alpha^4 n^4 \tilde{\phi}_n^\nu + i\alpha n R[(1-y^2-c_n^\nu)(\ddot{\tilde{\phi}}_n^\nu - \alpha^2 \tilde{\phi}_n^\nu) - 4y\dot{\tilde{\phi}}_n^\nu] = 0, \quad (15)$$

which satisfy the boundary conditions (14), have the same eigenvalues $c_n^\nu$, and meet the orthogonality condition (Eckhaus 1965)

$$\int_{-1}^{1} (\ddot{\phi}_n^\nu - \alpha^2 n^2 \phi_n^\nu)\tilde{\phi}_n^\sigma = \delta_{\nu\sigma}. \quad (16)$$

For the $\phi_n^\nu$ we adopt the normalization

$$\phi_n^\nu(y=0)=1, \tag{17}$$

while (16) in turn fixes the normalization of $\tilde{\phi}_n^\nu$.

In (2), let

$$f_1(y,t)=\sum_{\nu=1}^{\kappa} B_\nu(t)\,\phi_1^\nu(y), \tag{18}$$

$$f_2(y,t)=\sum_{\nu=1}^{\kappa} D_\nu(t)\,\phi_2^\nu(y), \tag{19}$$

$$f_3(y,t)=\sum_{\nu=1}^{\kappa} E_\nu(t)\,\phi_3^\nu(y). \tag{20}$$

Substituting (11) into (10) and equating Fourier coefficients, we get

$$\frac{dA_\sigma}{dt}=-\frac{\pi^2(\sigma-\frac{1}{2})^2}{R}A_\sigma-4\alpha\mathscr{I}\sum_{\nu=1}^{\kappa}\sum_{\tau=1}^{\kappa}[\bar{B}_\nu B_\tau\Gamma_{\sigma 1}^{\nu\tau}+2\bar{D}_\nu D_\tau\Gamma_{\sigma 2}^{\nu\tau}+3\bar{E}_\nu E_\tau\Gamma_{\sigma 3}^{\nu\tau}]. \tag{21}$$

where

$$\Gamma_{\sigma n}^{\nu\tau}=\int_0^1\cos[(\sigma-\tfrac{1}{2})\pi y]\,\bar{\phi}_n^\nu\,\tilde{\phi}_n^\tau\,dy. \tag{22}$$

Substituting now (18), (19) and (20) in (5) for $n=1$, 2 and 3 respectively, and making use of the orthogonality condition (16), we are led to the following system of equations for the determination of the functions $B_\nu(t)$, $D_\nu(t)$ and $E_\nu(t)$:

$$\frac{dB_\nu}{dt}=i\alpha c_1^\nu B_\nu+2i\alpha\sum_{\sigma=1}^{s}\sum_{\tau=1}^{\kappa}A_\sigma B_\tau Q_{\sigma 1}^{\nu\tau}+2i\alpha\sum_{l=1}^{\kappa}\sum_{j=1}^{\kappa}\bar{B}_l D_j V_{\nu lj}+2i\alpha\sum_{l=1}^{\kappa}\sum_{j=1}^{\kappa}\bar{D}_l E_j S_{\nu lj}, \tag{23}$$

$$\frac{dD_\nu}{dt}=2i\alpha c_2^\nu D_\nu+4i\alpha\sum_{\sigma=1}^{s}\sum_{\tau=1}^{\kappa}A_\sigma D_\tau Q_{\sigma 2}^{\nu\tau}+2i\alpha\sum_{l=1}^{\kappa}\sum_{j=1}^{\kappa}B_l B_j W_{\nu lj}+2i\alpha\sum_{l=1}^{\kappa}\sum_{j=1}^{\kappa}\bar{B}_l E_j U_{\nu lj}, \tag{24}$$

$$\frac{dE_\nu}{dt}=3i\alpha c_3^\nu E_\nu+6i\alpha\sum_{\sigma=1}^{s}\sum_{\tau=1}^{\kappa}A_\sigma E_\tau Q_{\sigma 3}^{\nu\tau}+2i\alpha\sum_{l=1}^{\kappa}\sum_{j=1}^{\kappa}B_l D_j T_{\nu lj}, \tag{25}$$

where

$$V_{\nu lj}=\int_0^1\tilde{\phi}_1^\nu[\bar{\phi}_1^l\dot{\gamma}_2^j-\bar{\gamma}_1^l\dot{\phi}_2^j+2\dot{\bar{\phi}}_1^l\gamma_2^j-2\dot{\bar{\gamma}}_1^l\phi_2^j]\,dy, \tag{26}$$

$$W_{\nu lj}=\int_0^1\tilde{\phi}_2^\nu[\phi_1^l\dot{\phi}_1^j-\phi_1^l\dot{\phi}_1^j]\,dy, \tag{27}$$

$$S_{\nu lj}=\int_0^1\tilde{\phi}_1^\nu[2\bar{\phi}_2^l\dot{\gamma}_3^j+3\dot{\bar{\phi}}_2^l\gamma_3^j-2\bar{\gamma}_2^l\dot{\phi}_3^j-3\dot{\bar{\gamma}}_2^l\phi_3^j]\,dy, \tag{28}$$

$$T_{\nu lj}=\int_0^1\tilde{\phi}_3^\nu[-2\dot{\gamma}_1^l\phi_2^j+\gamma_1^l\dot{\phi}_2^j-\phi_1^l\dot{\gamma}_2^j+2\dot{\phi}_1^l\gamma_2^j]\,dy, \tag{29}$$

$$U_{\nu lj}=\int_0^1\tilde{\phi}_2^\nu[3\dot{\bar{\phi}}_1^l\gamma_3^j-\bar{\gamma}_1^l\dot{\phi}_3^j-3\dot{\bar{\gamma}}_1^l\phi_3^j+\bar{\phi}_1^l\dot{\gamma}_3^j]. \tag{30}$$

$$\gamma_n^\nu=\ddot{\phi}_n^\nu-\alpha^2n^2\phi_n^\nu,$$

$$Q_{\sigma n}^{\nu\tau}=\int_0^1\tilde{\phi}_n^\nu\cos[(\sigma-\tfrac{1}{2})\pi y][\gamma_n^\tau+\pi^2(\sigma-\tfrac{1}{2})^2\phi_n^\tau]\,dy. \tag{31}$$

Equations (21), (23), (24) and (25) constitute a system of ordinary non-linear differential equations for the determination of the functions $A_\sigma(t)$, $B_\nu(t)$, $D_\nu(t)$ and $E_\nu(t)$, where $\sigma$ ranges from 1 to $s$ and $\nu$ from 1 to $\kappa$. We have solved this system using Nordsieck's method (Nordsieck 1963, p. 241). In this method, the size of the step of integration is regulated automatically during the course of integration so as to maintain a uniform accuracy of prescribed degree. The truncation limits adopted were $\kappa = 21$, $s = 60$. The results for $s = 30$ were close to those for $s = 60$.

## 3. Discussion of results

We have solved the system (23), (24) and (25) under the following initial conditions. For $t < 0$ we have the laminar plane Poiseuille flow, with the parabolic velocity profile as given in (1). At $t = 0$ we superimpose on the parabolic flow a disturbance periodic in $x$ and represented in (18) by the first mode ($\nu = 1$) only of the Orr–Sommerfeld equation, with an amplitude $\lambda$:

$$B_1(0) = \lambda, \tag{32}$$

$$B_\nu(0) = 0 \quad (\nu = 2, \ldots, \kappa). \tag{33}$$

The higher harmonics also vanish initially

$$D_\nu(0) = E_\nu(0) = 0 \quad (\nu = 1, 2, \ldots, \kappa). \tag{34}$$

It follows that the modification of the mean flow, as represented by $f_0$ in (11), also vanishes initially.

Figure 1 represents the development in time of disturbances, when the initial amplitude $\lambda$ in (32) is below the critical value $\lambda_c$, and the disturbance dies down. In the case of $\lambda = 0{\cdot}010$, represented by the dotted curves, the amplitude of the first mode $B_1(t)$ decays almost according to its own decrement $\exp(-c_{1i}^1 t)$, where $c_{1i}^1$ is the imaginary part of the first eigenvalue of the Orr–Sommerfeld equation (12). The only manifestation of non-linear effects is shown by the emergence of the curve $B_9$ at $t = 9{\cdot}0$ and its persistence above the threshold level of 0·001 until $t = 13{\cdot}6$. The curvature of the mean flow, which is given by $(2 - \bar{f}_0)$, varies by less than 10 % from its value of 2 in the laminar flow. The second case shown in figure 1, with $\lambda = 0{\cdot}013$, is just on the verge of the instability limit. Although $B_1(t)$ eventually decays with time, the quadratic terms in the hydrodynamic equations cause the excitation (from zero) of a host of higher order modes $B_\nu(t)$ in the expansion (18) for $f_1(y, t)$, as well as of some modes $D_\nu(t)$ in the expansion of the second harmonic function $f_2(y, t)$ in (19). At the height of the development of the secondary disturbance, the curvature of the mean flow even becomes negative, as is shown in figure 2. The profile of the mean velocity, however, does not deviate by more than about 1 % from the parabolic distribution. We note that nowhere in figure 1 do the coefficients $E_\nu(t)$ of $f_3(y, t)$ in (20) emerge above the 0·001 level.

For the higher value of $\lambda = 0{\cdot}014$ the disturbance is unstable, and the flow breaks down, as is shown in figure 3. In order not to obscure the graph we have

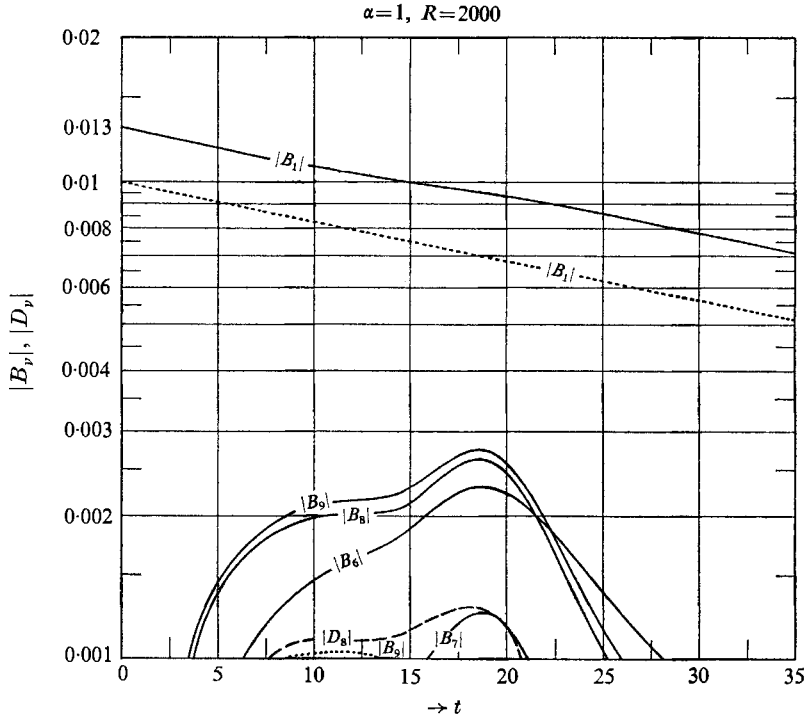


FIGURE 1. Variation with time of the coefficients in the expansions (18), (19) and (20). Initially, $B_1 = 0{\cdot}010$ and $0{\cdot}013$ respectively, and the other coefficients are zero. The motion is stable.

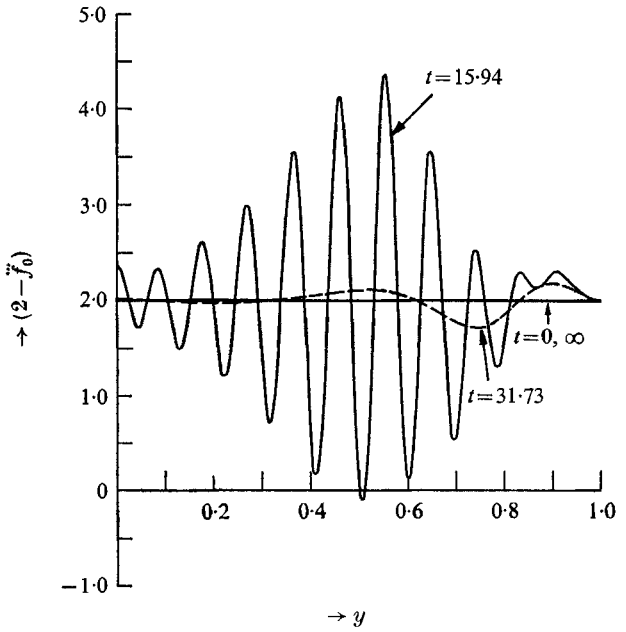


FIGURE 2. The profile of the curvature of the mean flow $(2-\ddot{f}_0)$ for the case $\lambda = 0{\cdot}013$ in figure 1. At $t = 0$ and at $t \to \infty, \ddot{f}_0 = 0$.

not entered in this figure some late-emerging modes from the $D_\nu$'s. Also omitted were some $E_\nu$'s which emerge after the appearance of $E_{11}$, $E_{12}$ and $E_{14}$. Not only are the coefficients $D_\nu(t)$ in the second harmonic function $f_2(y, t)$ excited, but also the coefficients $E_\nu(t)$ of the third harmonic function $f_3(y, t)$ in (20) begin to emerge

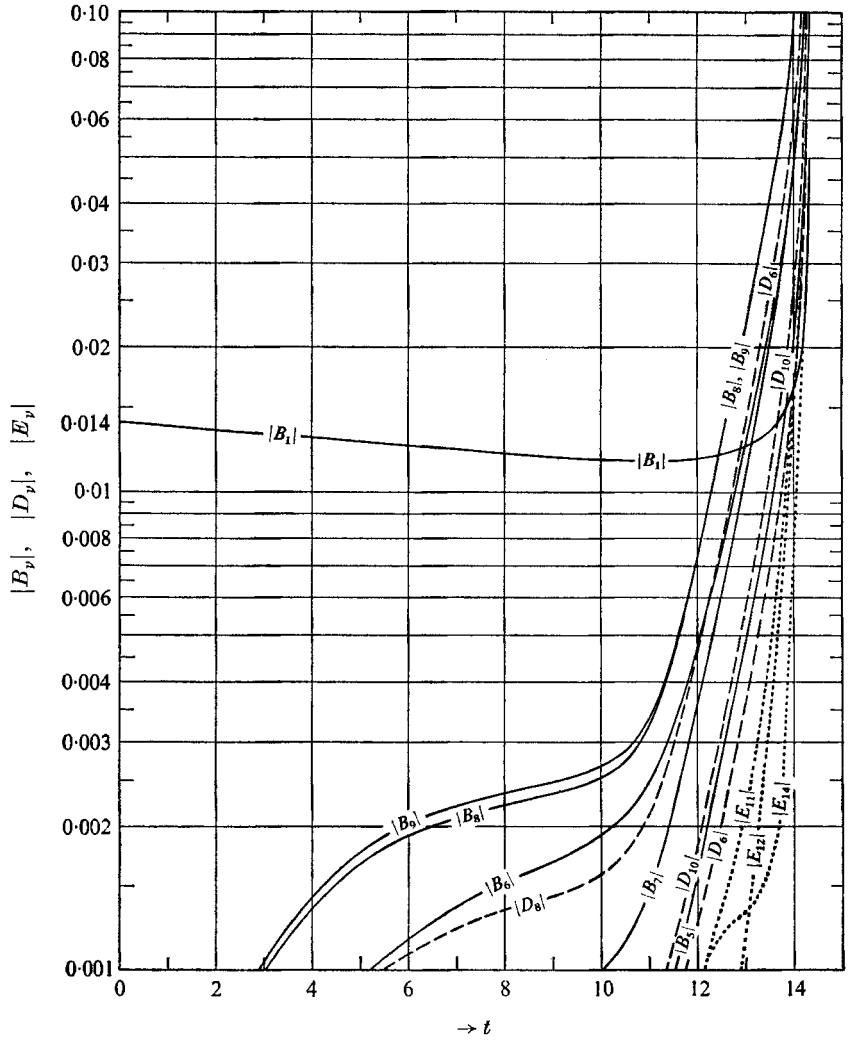


FIGURE 3. Variation with time of the coefficients in the expansions (18), (19) and (20) Initially $B_1(0) = 0{\cdot}014$, and all the others zero. The motion is unstable.

after $t = 12{\cdot}2$. When the latter become appreciable, our analysis no longer represents the real flow, since the truncation at $n = 3$ in the expansion (2) becomes of doubtful validity. Here the curvature becomes negative after $t = 10{\cdot}9$. Subsequently, many zones of negative curvature develop in the profile, but our analysis then becomes questionable.

The development of the instability shown in figure 3 is probably valid through $t = 13$. Thereafter, the third harmonic, given in (20), grows to a magnitude which begins to cast doubt on the justification for the neglect of the higher order harmonics. Even then, the cut-off at the 21st mode ($\nu = 21$) is still not manifestly violated, as evidenced by the rapid decrease of the coefficients for high values of $\nu$.

## 4. Excitation of the higher order modes

In the examples shown in figures 1 and 3, we start initially with a disturbance of the purely first mode, and subsequently find that there appear higher-order modes which are generated by self-excitation through the non-linear terms in the hydrodynamic equations. The way the higher order modes are excited seems to be peculiar. In the case of $\lambda = 0{\cdot}013$ shown in figure 1, it is the ninth-order mode $B_9$ of the first harmonic that is first excited. Similarly, in the unstable case of $\lambda = 0{\cdot}014$ in figure 3, it is the group $B_9$, $B_8$, $B_6$ and $B_7$ that is excited, and their first appearance is in that order. This phenomenon reflects an intrinsic structure of the eigenfunctions of the Orr–Sommerfeld equation which has not been recognized hitherto. Figure 4 gives the location of the eigenvalues $c_1^\nu$ of the first harmonic ($n = 1$) in the complex $c$ plane. The order-number $\nu$ has been assigned mostly according to the size of the imaginary part $c_{1i}^\nu$. We note that the eigenvalues group themselves into two classes, which later merge. In the first class, which includes modes of order $\nu = 1$, 3, and 6, the phase-velocity of the mode $c_{1r}^\nu$ is small, whereas in the second group, which lie along the sequence $\nu = 2, 4, 5, \ldots, c_{1r}^\nu$ is close to the maximum speed of 1 of the mean flow at the centre of channel. Even clearer separations into the two classes is shown in figures 10 and 12. We shall designate the first class as *boundary modes*, since they propagate with a speed appropriate to the neighbourhood of the wall in the parabolic flow, while the second class we shall designate as *interior modes*, since their speed of propagation is characteristic of the centre of the channel. The difference in the two classes of modes is brought out in figure 5, where we have plotted the absolute value of the vorticity $|\gamma_1^\nu|$ for the first and second modes in the case $\alpha = 1$, $R = 5000$. We note that in the first mode the vorticity $|\gamma_1^1|$ is concentrated near the wall, while in the second mode the vorticity $|\gamma_1^2|$ is concentrated near the centre of the channel. This localization is also characteristic of the respective phase-velocities shown by the arrows. In figure 6, the dashed curves are the vorticity functions for the interior modes, and the solid curves for the boundary modes, for the case $\alpha = 1$, $R = 2000$ shown in figure 4. The nodal characteristics of the higher order modes are illustrated in figure 8. It is seen that while the function $|\gamma_1^{12}|$ in figure 7 is dominated mainly by a single peak, the function $\gamma_1^{12}$ itself, shown in figure 8, has a complicated internal structure with many nodes characteristic of the high order of the mode. Similar high nodal features are shown by $\phi_1^5$ and $\phi_1^5$ in figure 9.

The most sensitive modes to be excited are $\nu = 8$ and 9 (figure 4), which lie in the $c$ plane at the junction of the two branches. Similarly, in the case of the second harmonic shown in figure 10, the most sensitive modes are $\phi_8^2$, $\phi_9^2$ and $\phi_{10}^2$, which are located at the junction of the two classes. In the third harmonic it is

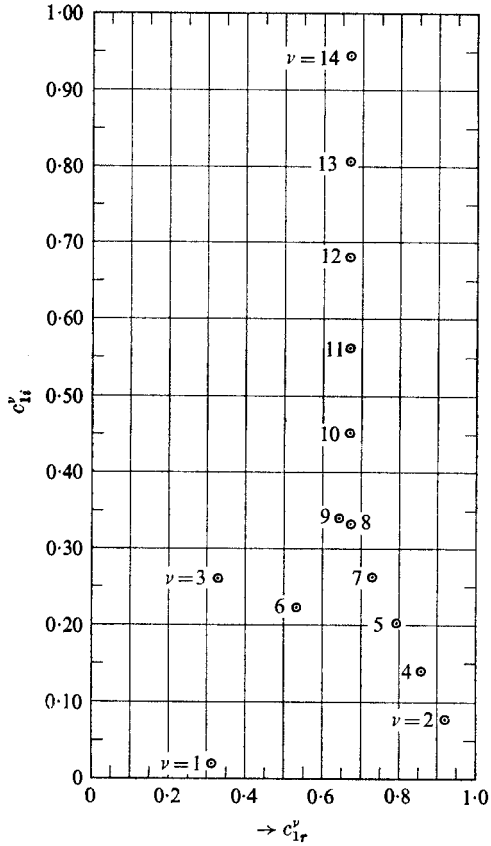


FIGURE 4. The eigenvalues $c_1^\nu = c_{1r}^\nu + ic_{1i}^\nu$ of the Orr–Sommerfeld equation (12) belonging to the first mode $n = 1$. $\alpha = 1$, $R = 2000$.

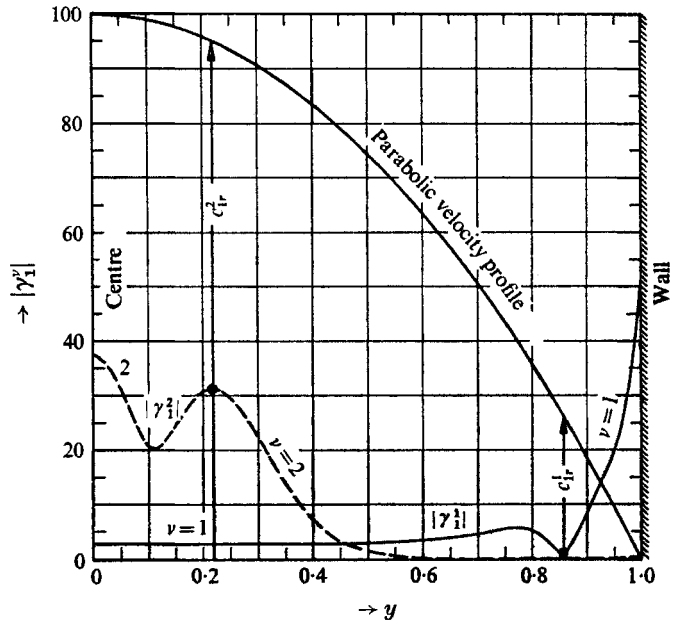


FIGURE 5. The profile of the absolute value of the vorticity $\gamma_n^\nu = \ddot{\phi}_n^\nu - \alpha^2\phi_n^\nu$ of the eigenfunctions of the first harmonic ($n = 1$). The arrows show the magnitude of the phase-velocity $c_{1r}^1$ and $c_{1r}^2$ of the first and second mode. $\alpha = 1$, $R = 5000$.

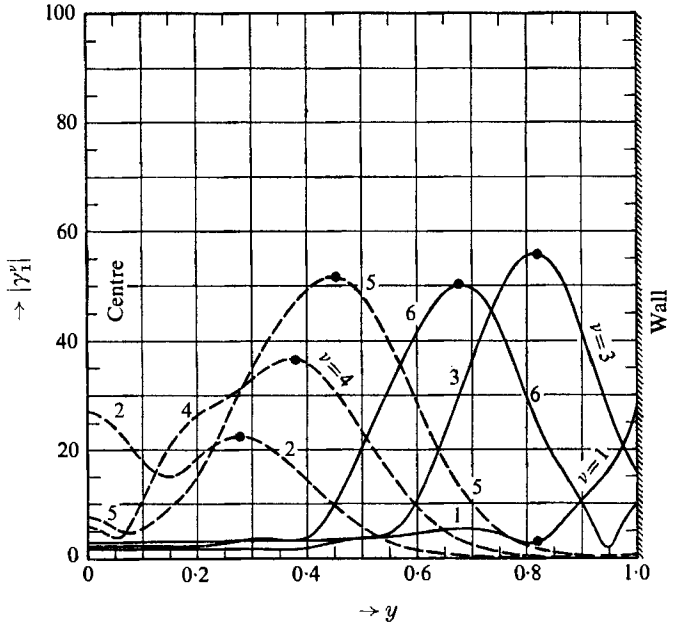


FIGURE 6. The distribution of the absolute value of the vorticity $|\gamma_1^\nu|$ for the modes shown in figure 4. $\alpha = 1$, $R = 2000$. The phase-velocity of each mode corresponds to the velocity in the parabolic flow of figure 5 at the co-ordinate $y$ of the dot.

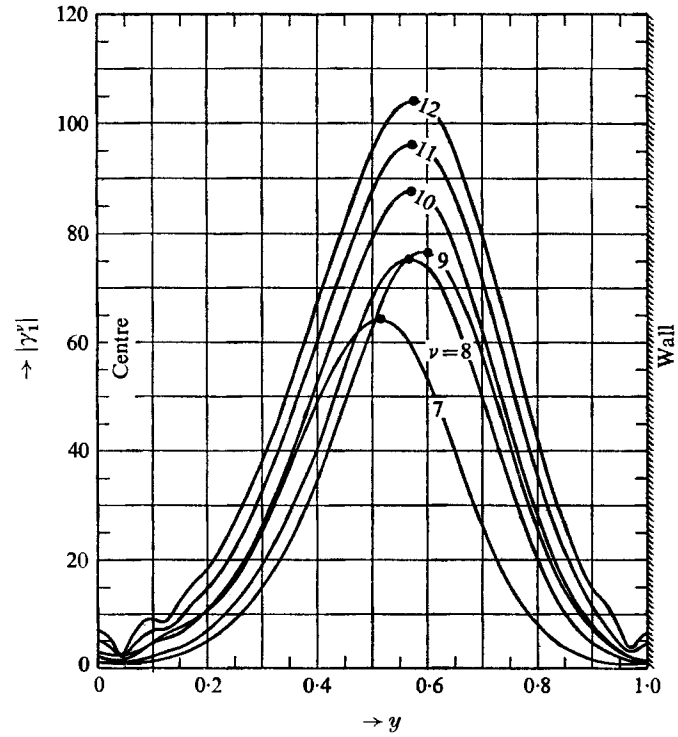


FIGURE 7. The merging of the vorticity functions $|\gamma_1^\nu|$ for the higher order modes of figure 4. $\alpha = 1$, $R = 2000$. The dots indicate the phase velocity at the corresponding position in the parabolic flow.

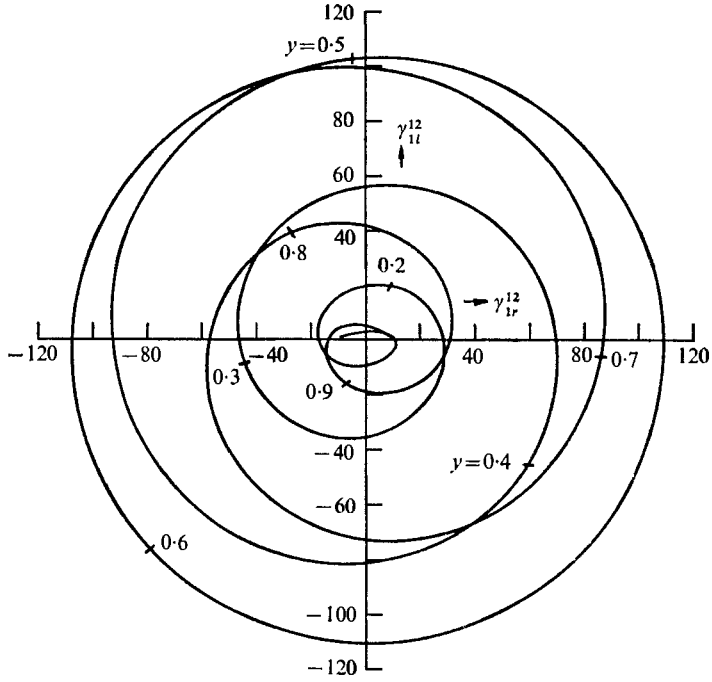


FIGURE 8. The function $\gamma_1^{12} = \gamma_{1r}^{12} + i\gamma_{1i}^{12}$ in its complex plane.
$\alpha = 1$, $R = 2000$.

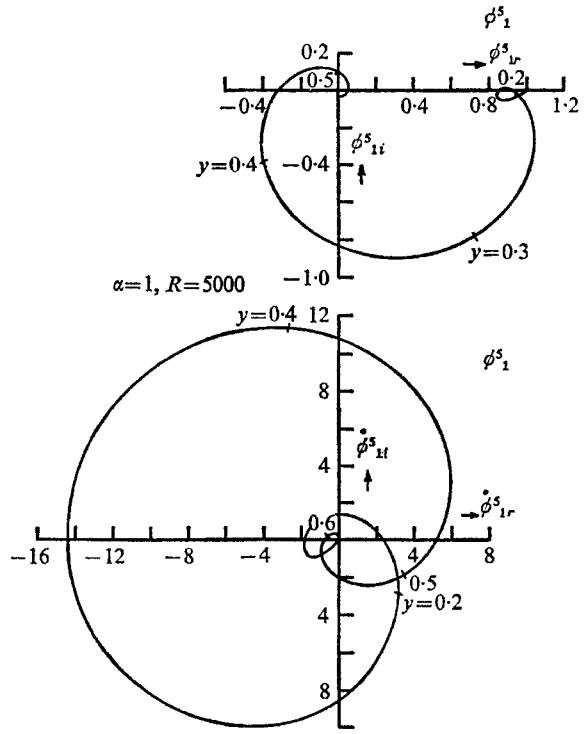


FIGURE 9. The eigenfunction $\phi_1^5$ and $\dot{\phi}_1^5$ in their respective complex planes.

$\phi_{14}^3$ which is similarly situated at the branching point, hence its emergence in figure 3. The oscillations in the curvature of the mean flow shown in figure 2 stem from the $B_8$ and $B_9$ modes.

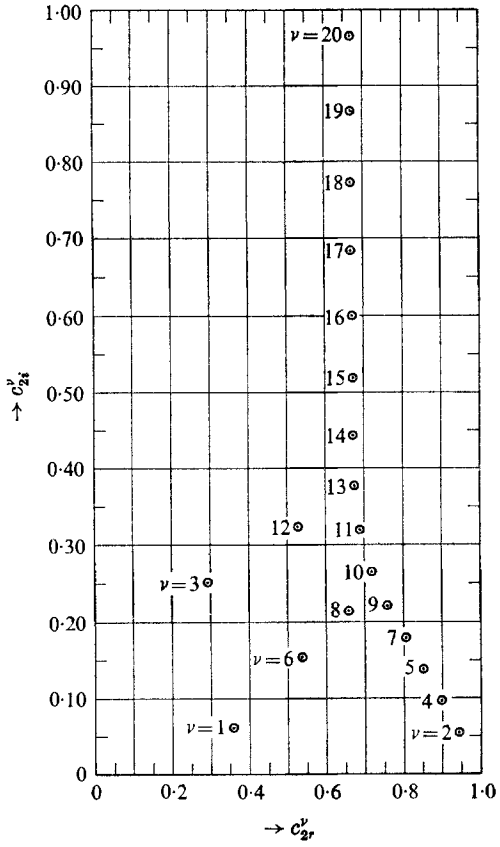


FIGURE 10. The eigenvalues $c_2^\nu = c_{2r}^\nu + ic_{2i}^\nu$ of the second harmonic ($n = 2$). $\alpha = 2$, $R = 2000$.

We have mapped out the critical amplitude $\lambda_c$ as a function of $R$ in the case when the initial disturbance is of the first mode.

The physical meaning of $\lambda$ derives from the condition that, at the time $t = 0$, the stream function $\psi$ in (2) is given by

$$\psi = (y - \tfrac{1}{3}y^3) + 2\lambda\,\mathscr{R}[\phi_1^1(y)\,e^{-i\alpha x}], \tag{35}$$

where $\phi_1^1(y)$ is the first even eigenfunction of the Orr–Sommerfeld equation, normalized so that $\phi_1^1(0) = 1$, and $\mathscr{R}$ denotes the real part. The fluctuating velocity-field imposed initially is derived from the term in brackets in (35). It has a distribution across the channel as in the first even mode of the Orr–Sommerfeld equation, and its amplitude is proportional to $\lambda$. When $\lambda$ exceeds the critical value $\lambda_c$, the initial disturbance causes the parabolic flow to break down after a certain time.

The results are shown in figure 11 for the case of $\alpha = 1$. $\lambda_c$ decreases monotonically with increasing $R$, becoming zero on the 'neutral curve', when $R = 5815$. Near $R = 5000$, the magnitude of the higher harmonics $f_n(y,t)$ in (18)–(20) decreases rapidly with increasing order $n$. The rate of decrease becomes less rapid as $R$ decreases, so that for $R < 1000$ our truncation limit of $n = 3$ is not manifestly sufficient. We therefore leave the question open as to whether, in the case of plane Poiseuille flow and the type of periodic disturbance we have assumed in this investigation, there exists a 'lower critical Reynolds number', below which any disturbance, of however large an amplitude, eventually dies down.

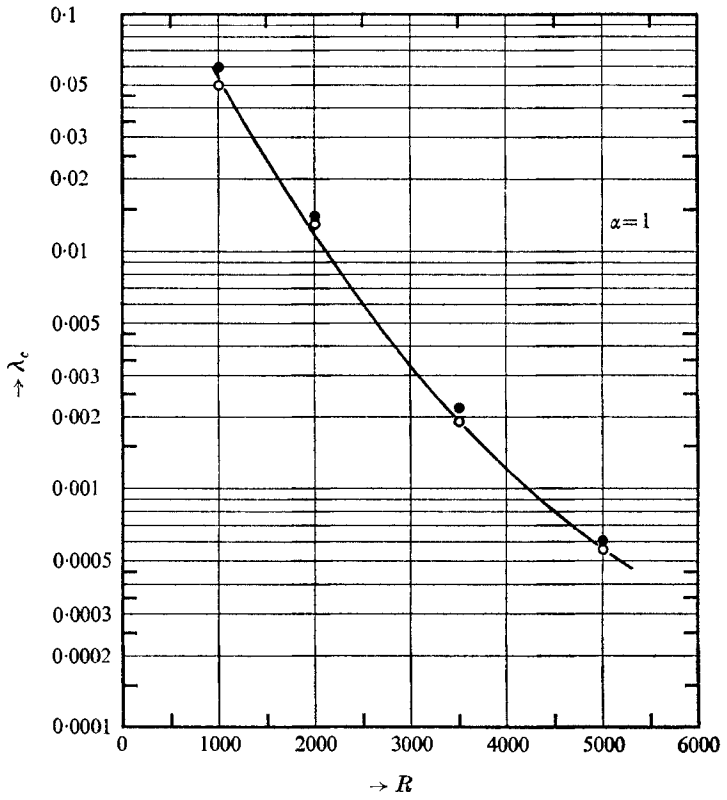


FIGURE 11. The critical value of the amplitude $\lambda_c$ as a function of the Reynolds number $R$, for the case of a disturbance represented by the first mode of the Orr–Sommerfeld equation. ●, unstable; ○, stable.

## 5. Initial disturbances belonging to the transition modes

Figure 12 gives the eigenvalues $c_1^{\nu}$ of the first harmonic for the case of $\alpha = 1$, $R = 5000$, showing the transition-zone at $\nu = 12$, 13, 14. When the initial disturbance is of the first mode, as in the previous discussion, with initial conditions given by (32), (33) and (34), the disturbance is still stable at an amplitude $\lambda = 0{\cdot}00055$, but the flow breaks down for $\lambda_c = 0{\cdot}00060$. The latter instability is shown in figure 13. We see that along with the imposed disturbance $B_1$, which

becomes unstable at $t = 13{\cdot}7$ when $(2-\ddot{f}_0)$ first becomes negative (figure 15), the modes in the transition zone $B_{12}$, $B_{13}$ and $B_{14}$ also build up to comparable magnitude even before instability sets in. We have accordingly studied the development of a disturbance which initially is purely $B_{12}$, with all the other

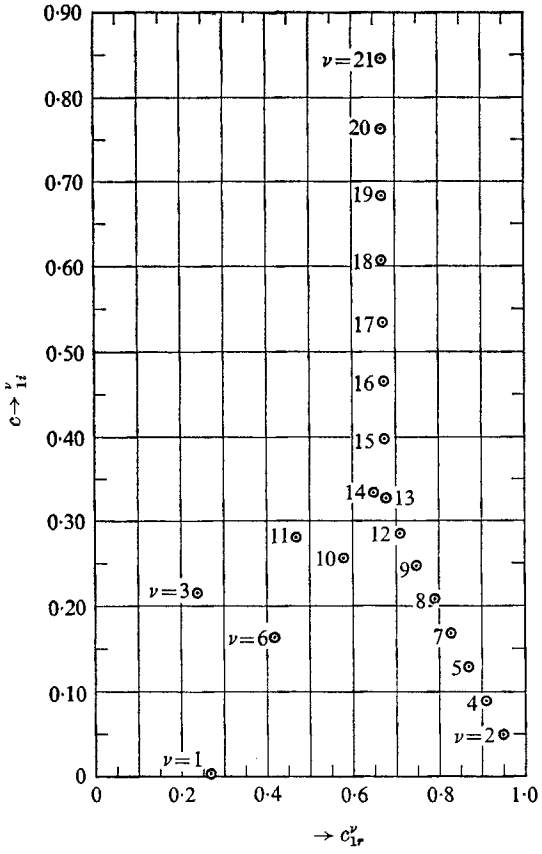


FIGURE 12. The eigenvalues $c_1^{\nu} = c_{1r}^{\nu} + ic_{1i}^{\nu}$ of the first harmonic ($n = 1$). $\alpha = 1$, $R = 5000$.

modes vanishing. The initial disturbance is therefore given by (35), with $\phi_1^1(y)$ replaced by $\phi_1^{12}(y)$. We find that at $\lambda = 0{\cdot}00010$ this disturbance dies down after building up comparable amplitudes in $B_{13}$ and $B_{14}$. When the initial value of $B_{12}$ is 0·00020 (as against 0·00060 above for a $B_1$-type excitation), the flow becomes unstable, as is shown in figure 14. We note again the excitation of the other modes 13 and 14 in the transition zone. These modes interfere mutually in their development and bring about a rhythmic pulsation superimposed on a growing disturbance-level, which resembles the mechanism of the breakdown of turbulence proposed by Landau (1944). However, the origin of the pulsation shown in figure 14, which is the merging of two types of modes, is different from the physical picture envisaged by Landau.

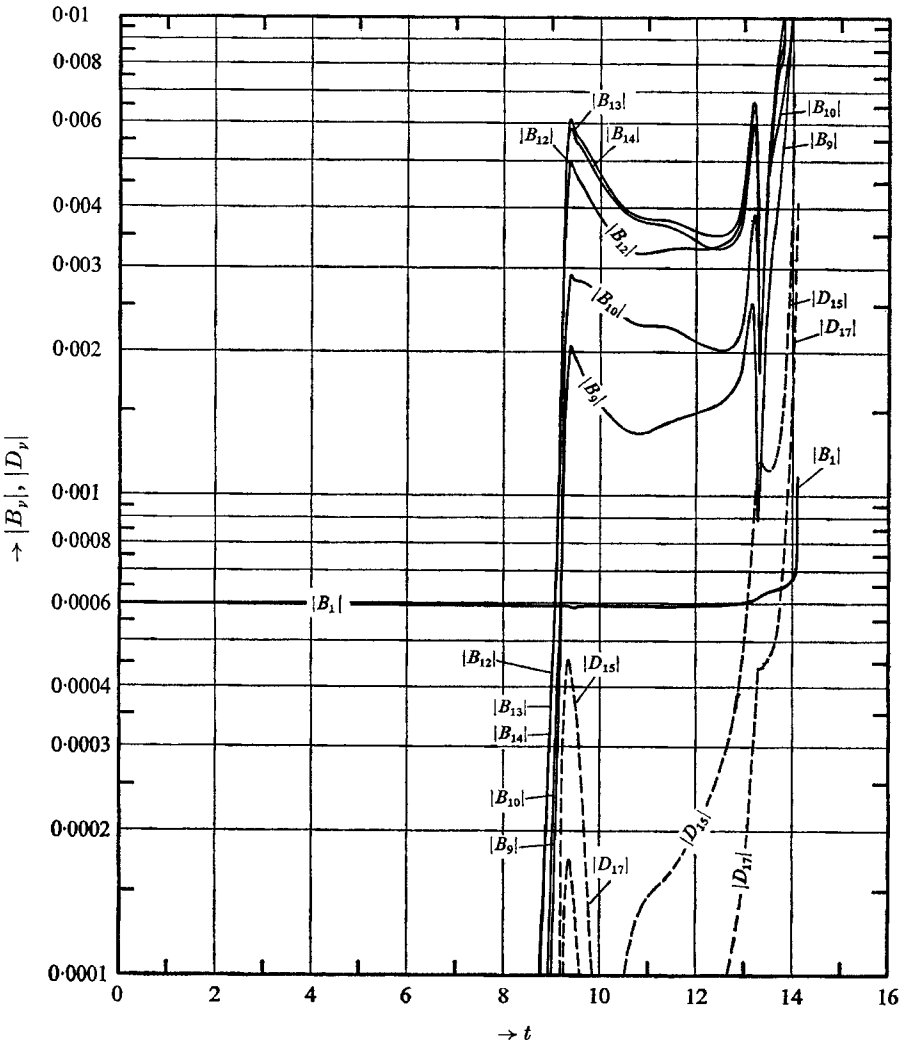


FIGURE 13. Development of a disturbance of the first mode, with an initial amplitude $B_1(0) = 0{\cdot}00060$. $\alpha = 1$, $R = 5000$.

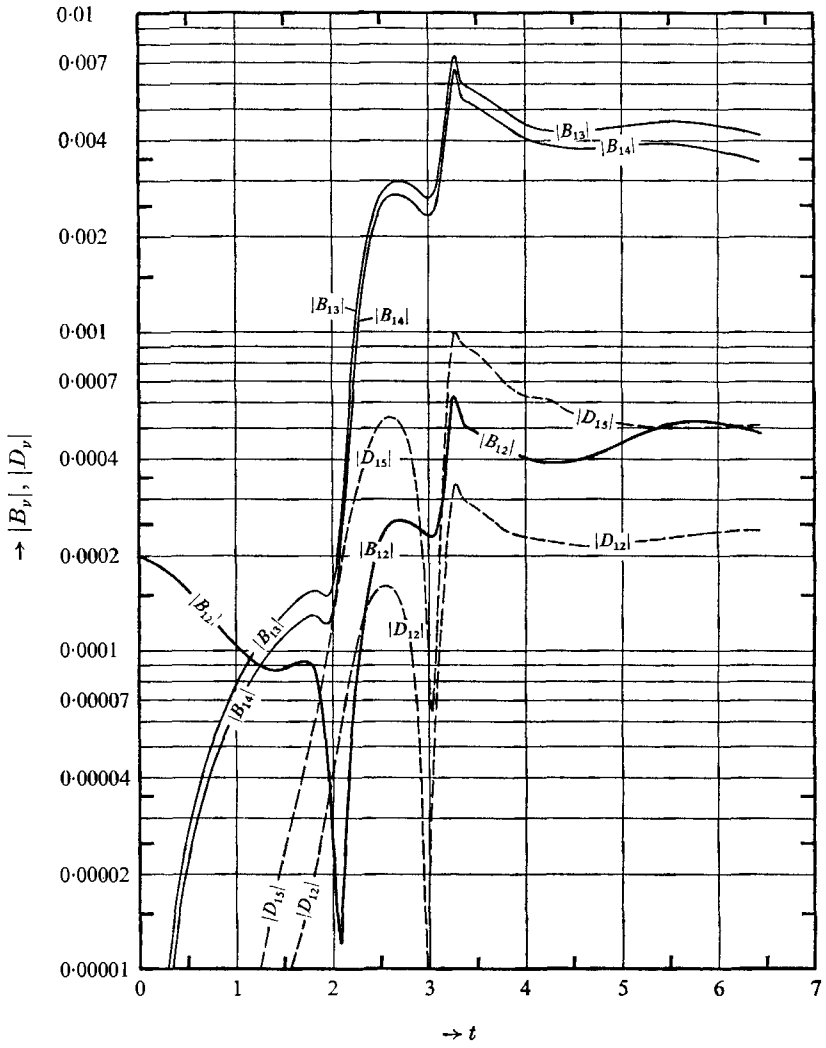


FIGURE 14. Development of a disturbance of the 12th mode, with initial amplitude $B_{12}(0) = 0{\cdot}00020$. $\alpha = 1$, $R = 5000$.

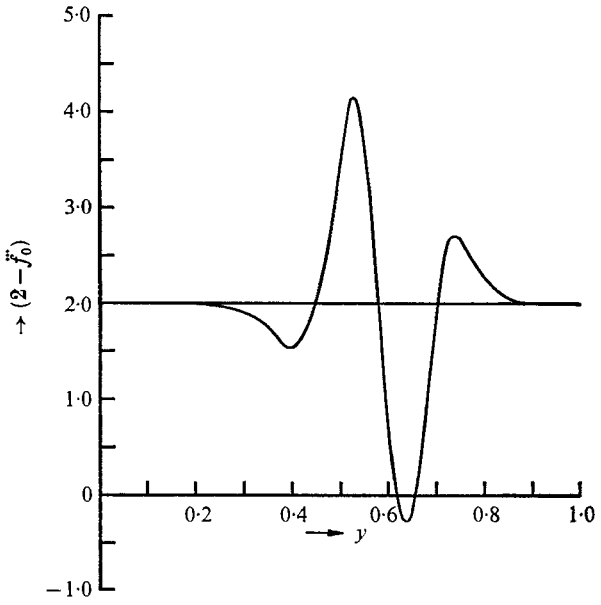


FIGURE 15. The curvature of the mean flow $(2-\bar{f}_0)$ shown in figure 13 at the time $t = 13{\cdot}7$, when it first becomes negative.

We are indebted to Mr Benjamin Gabai for assistance in programming. This investigation was supported by the National Science Foundation (Grant GP-8944).

## REFERENCES

ECKHAUS, W. 1965 *Studies in Non-Linear Stability Theory*. New York: Springer.

LANDAU, L. 1944 *C.R. Acad. Sci. U.R.S.S.* **44**, 311.

NORDSIECK, H. 1963 *Symposia in Applied Mathematics*. Providence: Am. Math. Soc.

STUART, J. T. 1960 *J. Fluid Mech.* **9**, 353.

WATSON, J. 1960 *J. Fluid Mech.* **8**, 371.